

## Numerical evidence of logarithmic regions in channel flow at $\text{Re}_\tau = 8000$

Yoshinobu Yamamoto\*

*Department of Mechanical Engineering, University of Yamanashi, 4-3-11, Takeda, Kofu 400-8511, Japan*

Yoshiyuki Tsuji†

*Department of Energy Science and Engineering, Nagoya University, Furo, Chikusa, Nagoya 464-8601, Japan*



(Received 3 August 2017; published 29 January 2018)

Direct numerical simulations of channel flow up to  $\text{Re}_\tau = 8000$  have been performed to determine the existence of a logarithmic region in channel flow at high-Reynolds number. It is notable that the logarithmic variations both in the mean velocity,  $U^+ = (1/\kappa) \ln(y^+) + B$  and the streamwise Reynolds stress,  $\overline{u^+u^+} = B_1 - A_1 \ln(y/h)$  are first confirmed for  $\text{Re}_\tau = 8000$ , with  $\kappa = 0.387$ ,  $B = 4.21$  and  $A_1 = 1.65$ ,  $B_1 = 1.23$ , where  $y$  is the distance from the wall and  $h$  is the channel half-height. The logarithmic region of  $U^+$  locates between  $300 < y^+ < 1100$  ( $y/h = 0.14$ ) and that of  $\overline{u^+u^+}$  locates between  $1200$  ( $y/h = 0.15$ )  $< y^+ < 2000$  ( $y/h = 0.25$ ). Therefore, these logarithmic regions do not overlap with each other. Furthermore, the region of  $k_x^{-1}$  law is studied without using the frozen turbulence hypothesis in logarithmic regions of the mean velocity and the streamwise Reynolds stress.

DOI: [10.1103/PhysRevFluids.3.012602](https://doi.org/10.1103/PhysRevFluids.3.012602)

### I. INTRODUCTION

In this study, we focus on the logarithmic regions of the streamwise mean velocity and the streamwise Reynolds stress in channel flow at a relatively high Reynolds number. The logarithmic relation of streamwise mean velocity as the result of the overlap between the inner small scales and outer large scales was first noted by Millikan [1] as

$$U^+ = \frac{1}{\kappa} \ln(y^+) + B, \quad (1)$$

where  $U$  is the mean velocity,  $y$  is the distance from the wall,  $\kappa$  is called the von Kármán constant,  $B$  is an additive constant, and superscript  $+$  denotes the nondimensional quantity normalized by friction velocity ( $u_\tau$ ) and kinematic viscosity ( $\nu$ ). The Kármán constant in channel flow was estimated as 0.37 [2] and 0.39 [3] by experiment, and was calculated as  $0.384 \pm 0.004$  [4] by direct numerical simulation (DNS) as well.

With regard to streamwise Reynolds stress, Townsend [5] and Perry *et al.* [6] suggested a sufficiently high-Reynolds-number presupposition that the logarithmic variation in streamwise (and spanwise) Reynolds stress has a log-law relation as Eq. (1), which is

$$\overline{u^+u^+} = B_1 - A_1 \ln(y/h), \quad (2)$$

where  $u$  is the streamwise velocity fluctuation,  $h$  is the boundary-layer thickness (or channel half-height, or pipe radius),  $A_1$  is the Townsend-Perry constant,  $B_1$  is an additive constant, and the overbar denotes the averaged value. This logarithmic variation is derived by the attached-eddy hypotheses

\*yamamotoy@yamanashi.ac.jp

†c42406a@nucc.cc.nagoya-u.ac.jp

[5,7] and the  $k_x^{-1}$  law [6] for the energy spectrum of the streamwise turbulent velocity, where  $k_x$  is the streamwise wave number. In pipe flow, Hultmark *et al.* [8] for the first time confirmed the logarithmic variation of  $\overline{u^+u^+}$  at the region where it overlaps with that of  $U^+$ ; the values of  $A_1$  and  $B_1$  are 1.25 and 1.61, respectively. In addition, Marusic *et al.* [9] supported the existence of a universal logarithmic region, where both the mean velocities and streamwise Reynolds stresses followed logarithmic functions of distance from the wall in the Reynolds number range of  $2 \times 10^4 < \text{Re}_\tau < 6 \times 10^5$  for boundary layers, pipe flow, and the atmospheric surface layer. Here,  $\text{Re}_\tau$  is the friction Reynolds number based on the friction velocity and the boundary-layer thickness (or pipe radius).

In contrast, Agostini and Leschziner [10] argued the discrepancy of wall-normal heights between logarithmic variations of  $\overline{u^+u^+}$  and  $U^+$  using the DNS database for channel flow at  $\text{Re}_\tau = 4200$  [11]. However, the logarithmic variation of  $\overline{u^+u^+}$  cannot be strictly displayed at  $\text{Re}_\tau = 4200$  [11] and 5200 [4] in channel flow. From the measurement in boundary layers [12–14], we assume that the sufficient scale separation between near-wall structures and large-scale structures in the premultiplied spectrum is substantialized for  $\text{Re}_\tau > 7000$ . In fact, Agostini and Leschziner [10] described that the streamwise Reynolds stresses tended to establish a logarithmic decay for  $\text{Re}_\tau > 7000$  in the experimental data by Hutchins *et al.* [13], Hultmark *et al.* [8,15], and Rosenberg *et al.* [16]. Therefore,  $\text{Re}_\tau = 7000$  might be the lowest possible Reynolds number to study the logarithmic variation of  $\overline{u^+u^+}$  by means of the DNS approach. In this study, we performed DNSs of fully developed channel flow up to  $\text{Re}_\tau = 8000$ . As a result, the logarithmic variations both in the mean velocity and the streamwise Reynolds stress in channel flow were confirmed. See Ref. [17] for the current DNS statistics.

## II. DNS PROCEDURES AND NUMERICAL CONDITIONS

In the following section, the streamwise ( $x$ ), wall-normal ( $y$ ), and spanwise ( $z$ ) turbulent velocities are denoted as  $u$ ,  $v$ , and  $w$ , respectively, with the mean velocity indicated by a capital letter.

The reported target flow is assumed to be a fully developed turbulent channel flow driven by the constant mean pressure gradient in the streamwise direction. DNSs of the incompressible Navier-Stokes equation are performed by the tenth-order accurate finite-difference method (tenth FD), which is proposed by Morinishi *et al.* [18] for the stream- and spanwise directions, and by the second-order finite-difference method (second FD) for the wall-normal direction on the full-staggered grid systems. Time advancement is carried out by the Euler implicit scheme for the pressure term and the second-order Adams-Bashforth scheme for the others, combined in the fractional-step procedure. The pressure Poisson equation is directly solved by using a two-dimensional fast Fourier transform for stream- and spanwise directions and a tridiagonal matrix algorithm for the wall-normal direction.

To detect the wavelength corresponding to  $6\delta$  (where  $\delta = h$  is the boundary-layer thickness) of the second peak in the streamwise premultiplied spectrum [12,13,16,19], the streamwise ( $x$ ) computational domain size in all cases is applied as  $16h$ , where  $h$  is the channel half-height.

In a full turbulence simulation, the grid spacing corresponding to the resolution of the Kolmogorov wave number ( $1/\eta$ ) is required. In the current DNS, we ensured over twice finer resolution compared to the Kolmogorov wave number in the wall-normal direction:

$$\frac{2\pi}{2\Delta y} > \frac{2}{\eta}. \quad (3)$$

In contrast, the coarser grid resolutions than the Kolmogorov wave number have been adapted in wall-parallel directions, which has been the case since the first DNS of channel flow reported by Kim *et al.* [20]:  $\Delta x^+ \approx 12$  and  $\Delta z^+ \approx 7$ . In the pseudospectral method adapted by previous DNS studies [4,11,21–26], the effective spatial resolutions in the wall-parallel directions are in the ranges from  $\Delta x^+ = 9$  [4,23] to 22 [21] in the streamwise direction, and from  $\Delta z^+ = 5$  [4] to 11 [21] in the spanwise direction. To adapt the tenth FD for wall-parallel directions, a grid-sensitivity analysis was conducted for the case of  $\text{Re}_\tau = 1000$  [27,28].

From the results of this grid-sensitivity analysis [28], current DNS conditions of up to  $\text{Re}_\tau = 8000$  are decided. In these conditions, the underestimation of the streamwise turbulent intensity affected

TABLE I. Summary of simulation conditions. Here,  $\text{Re}_\tau = u_\tau h/\nu$ , friction Reynolds number;  $u_\tau$ , friction velocity;  $h$ , channel half width;  $\nu$ , kinematic viscosity;  $U_b$ , bulk mean velocity;  $L_x$ , streamwise computational length;  $L_z$ , spanwise computational length;  $N_x(\Delta x)$ ,  $N_y(\Delta y)$ ,  $N_z(\Delta z)$ , grid number (resolution) for stream ( $x$ ), vertical ( $y$ ), and spanwise ( $z$ ) directions, respectively. 10th/2nd FD denotes tenth ( $x, z$ )- and second ( $y$ )-order accurate finite-difference method; SB denotes spectral ( $x, z$ ) and  $B$ -spline ( $y$ ) method; SC denotes spectral ( $x, z$ ) and compact finite-difference ( $y$ ) method; and 2nd FD denotes second-order accurate finite-difference method in all directions.

Name (method)	$\text{Re}_\tau$	$U_b^+$	$L_x/h$	$L_z/h$	$N_x(\Delta x^+)$	$N_y(\Delta y^+)$	$N_z(\Delta z^+)$	$T^+/\text{Re}_\tau$
YT1000 (10th/2nd FD)	1000	19.9	16.0	6.4	1440 (11.1)	512 (0.6–8.0)	768 (8.3)	12.0
YT2000 (10th/2nd FD)	1997	21.8	16.0	6.4	2880 (11.1)	1024 (0.6–8.0)	1536 (8.3)	10.0
YT4000 (10th/2nd FD)	3986	23.4	16.0	6.4	5760 (11.1)	2048 (0.6–8.0)	3072 (8.3)	9.0
YT8000C (10th/2nd FD)	8016	25.0	16.0	6.4	8640 (14.8)	4096 (0.6–8.0)	6144 (8.3)	6.3
LM1000 [4] (SB)	1000	20.0	$8\pi$	$3\pi$	2304 (10.9)	512 (0.02–6.2)	2048 (4.6)	12.5
HJ2000 [24] (SC)	2003	21.8	$8\pi$	$3\pi$	4096 (12.3)	633 (0.3–8.9)	3072 (6.1)	10.3
BPO2000 [25] (2nd FD)	2020	21.5	$6\pi$	$2\pi$	4096 (9.3)	768 (0.03–8.3)	2048 (6.1)	26.9
LJ4200 [11] (SC)	4179	23.5	$2\pi$	$\pi$	2048 (12.8)	1081 (0.3–10.7)	2048 (6.4)	15.0
BPO4100 [25] (2nd FD)	4079	23.2	$6\pi$	$2\pi$	8192 (9.4)	1024 (0.01–12.5)	4096 (6.2)	8.5
LM5200 [4] (SB)	5186	24.1	$8\pi$	$3\pi$	10240 (12.7)	1536 (0.5–10.3)	7680 (6.4)	7.8

by the spatial resolution was observed, in particular, for the wall-normal heights between  $y^+ = 10$  to 50. However, the streamwise premultiplied spectrum of  $u$ , which is one of the most primary statistics in high Reynolds number effects on wall turbulence, does not appear to be affected by the wall-parallel resolution. As such, the current DNS conditions can be reliably applied in the present study for investigating the mean velocity and the streamwise Reynolds stress related to large-scale structures in high Reynolds number conditions. The current DNS conditions are summarized in Table I, where  $T$  denotes the time-integration length to obtain the turbulent statistics, and  $\Delta x, \Delta y$ , and  $\Delta z$  are the grid resolutions for the streamwise, wall-normal, and spanwise directions. Moreover, the case names are named following Lee and Moser [4]. In Table I, previous high-Reynolds-number DNSs [4, 11, 25, 26] of channel flow are used as the reference data. The simulation at  $\text{Re}_\tau = 8000$  have been initiated with the rough-resolution DNS field [29] at the total time-integration point  $T^+/\text{Re}_\tau = 8.0$  with spatial resolutions of  $\Delta x^+ = 17.8$ ,  $\Delta y^+ = 0.6\text{--}8.0$ , and  $\Delta z^+ = 8.9$ . After the initial run ( $T^+/\text{Re}_\tau = 3.5$ ) to converge the effects of the changes in the spatial resolutions, the production run ( $T^+/\text{Re}_\tau = 6.3$ ) was conducted to obtain the turbulent statistics. This time-integration length of the production run corresponds to ten washout times, where one washout time is defined as the time taken by a fluid particle with the mean velocity at the centerline to cross the streamwise computational box ( $L_x = 16h$ ). In a steady-state fully developed channel flow, the total shear stress shows a liner profile as a function of the wall-normal height ( $y$ ) as

$$1 - \frac{y^+}{\text{Re}_\tau} = -\overline{u^+v^+} + \frac{dU^+}{dy^+}, \quad (4)$$

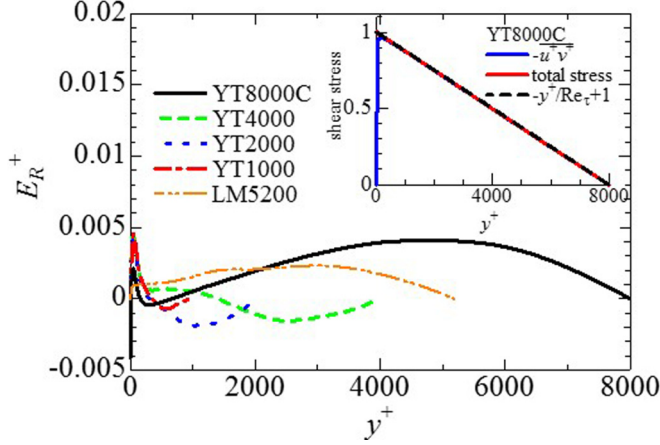


FIG. 1. Verification of statistical convergence; total shear balance (YT8000C), and residual of total shear stress for all cases.

where  $-\overline{u^+v^+}$  denotes the Reynolds shear stress. To check statistical errors in DNS data, Thompson *et al.* [30] used the following residual in shear stress balance:

$$E_R(y^+) = 1 - \frac{y^+}{\text{Re}_\tau} + \overline{u^+v^+} - \frac{dU^+}{dy^+}. \quad (5)$$

Figure 1 shows the shear stress profiles in YT8000C and residuals ( $E_R$ ) for all cases. The total shear stress profile in YT8000C shows a linear profile and  $E_R$  of the current DNS database is less than 0.05. From these results, time-integration lengths of the current DNS database are judged to be larger than the least length to satisfy the stably turbulent statistics.

### III. LOGARITHMIC VARIATION OF STREAMWISE MEAN VELOCITY AND REYNOLDS STRESS

Figures 2(a) and 2(b) show the indicator function  $\beta = y^+ dU^+/dy^+ (= 1/\kappa)$  and the test function of Townsend's prediction  $\Xi = y^+ d\overline{u^+u^+}/dy^+ (= -A_1)$ , where plateau regions denote

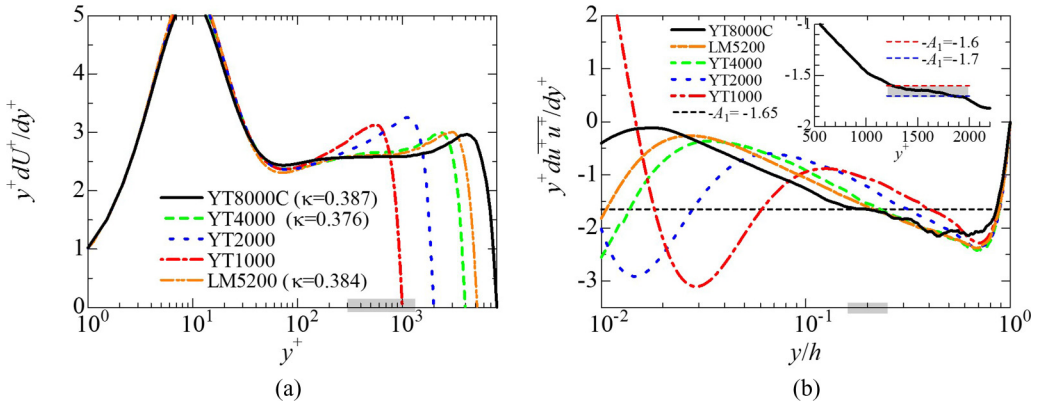


FIG. 2. Logarithmic variations of mean velocity and streamwise Reynolds stress. Darker-shaded regions denote the logarithmic regions in YT8000C. (a) Mean velocity: indicator parameter  $\beta (= 1/\kappa)$  and (b) streamwise Reynolds stress: test function  $\Xi (= -A_1)$ .

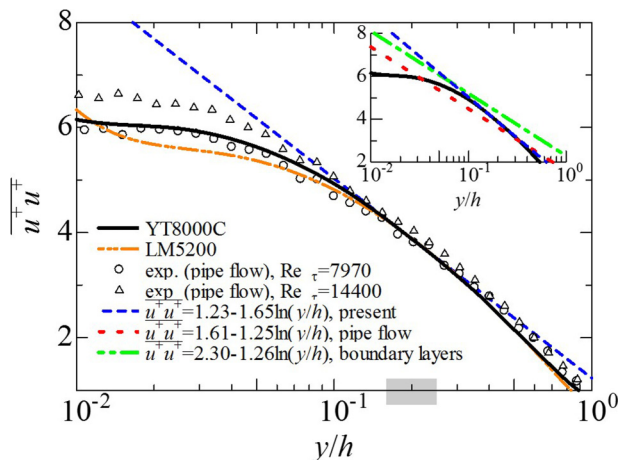


FIG. 3. Comparison with fitting equation of logarithmic variation in streamwise Reynolds stress and the current DNS in YT8000C and the experiments of pipe flow [30,31]. Darker-shaded region denotes the logarithmic region in YT8000C.

the logarithmic regions. In mean velocity profiles, logarithmic regions appeared in  $Re_\tau \geq 4000$ . In YT4000, the indicator function  $\beta$  is 2.658 between  $500 < y^+ < 800$  ( $y/h = 0.2$ );  $\beta$  is estimated by the least-squares approximation with the error of mean square =  $4.33 \times 10^{-6}$ . In the same way,  $\beta$  is 2.583 between  $300 < y^+ < 1100$  ( $y/h = 0.14$ ) with the error of mean square =  $2.85 \times 10^{-5}$  in YT8000C. Thereby, the Kármán constant and the additive constant of Eq. (1) is  $\kappa = 0.376$  and  $B = 3.89$  for YT4000, and  $\kappa = 0.387$  and  $B = 4.21$  for YT8000C. Lee and Moser [4] reported  $\kappa = 0.384 \pm 0.004$  and  $B = 4.27$  between  $350 < y^+ < 830$  ( $y/h = 0.16$ ) for LM52000. The experimental results are 0.37 [2] and 0.39 [3] in channel flow. The DNS results, thus, are consistent with the experimental results.

On the other hand, the test function  $\Xi$  shows the plateau region, that is equivalent to the logarithmic behavior of Eq. (2), is present only for the case of YT8000C. The wall-normal range is between  $1200$  ( $y/h = 0.15$ )  $< y^+ < 2000$  ( $y/h = 0.25$ ), and the Townsend-Perry constant [5,7] is estimated as  $A_1 = 1.65$  with the error of mean square =  $1.48 \times 10^{-3}$ . The additive constant of Eq. (2) is also estimated as  $B_1 = 1.23$ . Therefore, the present coefficients  $A_1$  and  $B_1$  have the certain differences with those of experimental results [8,9].

In comparison with the logarithmic region of the mean velocity, as shown in Fig. 2(b),  $\Xi$  has the steep gradient at  $y^+ < 1100$ , where the mean velocity has the logarithmic variation. Hence, the logarithmic variations of the mean velocity and the streamwise Reynolds stress cannot be confirmed at the same location.

Figure 3 shows the comparison of the streamwise Reynolds stress with experimental results in pipe flow [31,32], with the fitting equation suggested for pipe flow and boundary layers by Hultmark *et al.* [8] and Marusic *et al.* [9], respectively. As reported by Ng *et al.* [33], the streamwise Reynolds stress indicates similar statistical features in both pipe and channel flows. They checked this similarity in relatively low Reynolds number ( $Re_\tau < 3000$ ), but it may be expected in higher Reynolds number. The profile of YT8000 agrees reasonably well with the experimental data in pipe flow at  $Re_\tau = 7970$  [31,32]. When compared with the fitting equation for pipe flow at  $Re_\tau = 98190$  by Hultmark *et al.* [8], the logarithmic variation for YT8000C has a large difference as mentioned above in the Townsend-Perry constant because of the wall-normal height of the logarithmic regions. The log-arithmetic regions in YT8000C and experiments [31,32] are located around  $y/h \approx 0.2$ . By contrast, Hultmark *et al.* [8] and Marusic *et al.* [9] reported that the logarithmic regions are located around  $y/h \approx 0.1$ . This difference may be caused by the Reynolds number effects. In fact, the

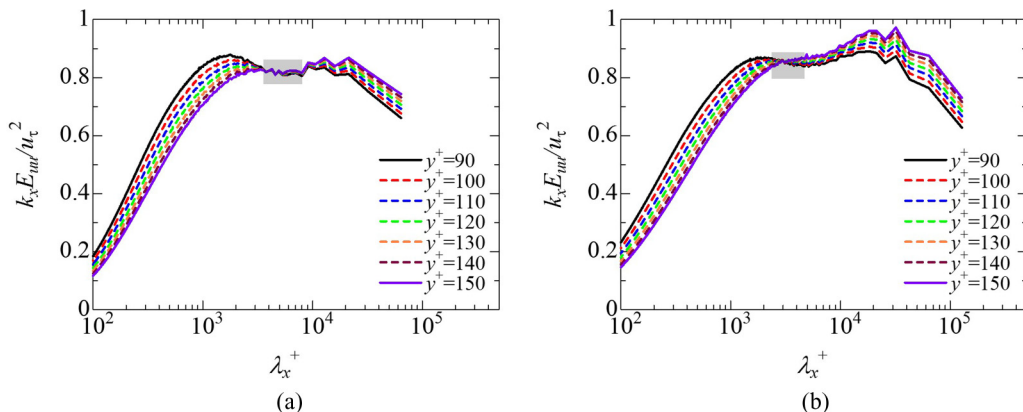


FIG. 4. Streamwise premultiplied spectrum of  $u$  at overlap region:  $90 < y^+ < 150$ . Darker-shaded regions denote the  $k_x^{-1}$  regions. (a)  $Re_\tau = 4000$  (YT4000) and (b)  $Re_\tau = 8000$  (YT8000C).

streamwise Reynolds stress of  $Re_\tau = 14400$  in experiment [31,32] extends its logarithmic region closer to the wall. Moreover, the fitting equation for the boundary layer at  $Re_\tau = 18010$  by Marusic *et al.* [9] comes near the profile of YT8000C.

#### IV. $k_x^{-1}$ LAW

Figure 4 shows the streamwise premultiplied spectra of  $u$  in YT4000 and YT8000C. The region is limited to  $90 < y^+ < 150$ , where Nickels *et al.* [34] confirmed the  $k_x^{-1}$  law. In this study, the streamwise premultiplied spectrum of  $u$ :  $k_x E_{uu}$  is defined as follows:

$$\overline{uu} = \int_0^\infty k_x E_{uu}(k_x) d\{\ln(k_x)\}. \quad (6)$$

Here  $k_x (= 2\pi/\lambda_x, \lambda_x$  is the streamwise wavelength) is the streamwise wave number. As illustrated in Fig. 4, the regions of the  $k_x^{-1}$  law are marked as the darker-shaded squares.

In each case, the first peak is observed at  $\lambda_x^+ \approx 1000$ – $2000$  which is caused from the near-wall cycle of streaks and quasistreamwise vortices [35–37]. Besides, the weak second peak appears at  $\lambda_x^+ \approx 10000$  in YT2000 (not shown). With increasing of  $Re_\tau$ , this second peak shifts from  $\lambda_x^+ \approx 10000$  to the longer wavelength, and its amplitude becomes larger than the first peak in YT8000C. Consequently, the region of the  $k_x^{-1}$  law is clearly observed in YT4000 but it becomes narrower in YT8000C. These tendencies are consistent with experimental result [16] and DNS [4]. It is hard to observe the clear long-range  $k_x^{-1}$  law region even in the present Reynolds number. This reason is argued as the results from the finite value of Reynolds number and aliasing problem associated with one-dimensional spectra by Davidson *et al.* [38].

TABLE II. Wavelengths of peaks in the premultiplied spectrum at the overlap region:  $90 < y^+ < 150$ .

$Re_\tau$	First peak			Second peak		
	$k_x h$	$\lambda_x^+$	$\lambda_x/h$	$k_x h$	$\lambda_x^+$	$\lambda_x/h$
1000	4.7	1337	1.3			
2000	8.6	1461	0.7	1.2	10472	5.2
4000	14.5	1733	0.4	1.2	21481	5.4
8000	27.5	1828	0.2	1.6	32016	4.0

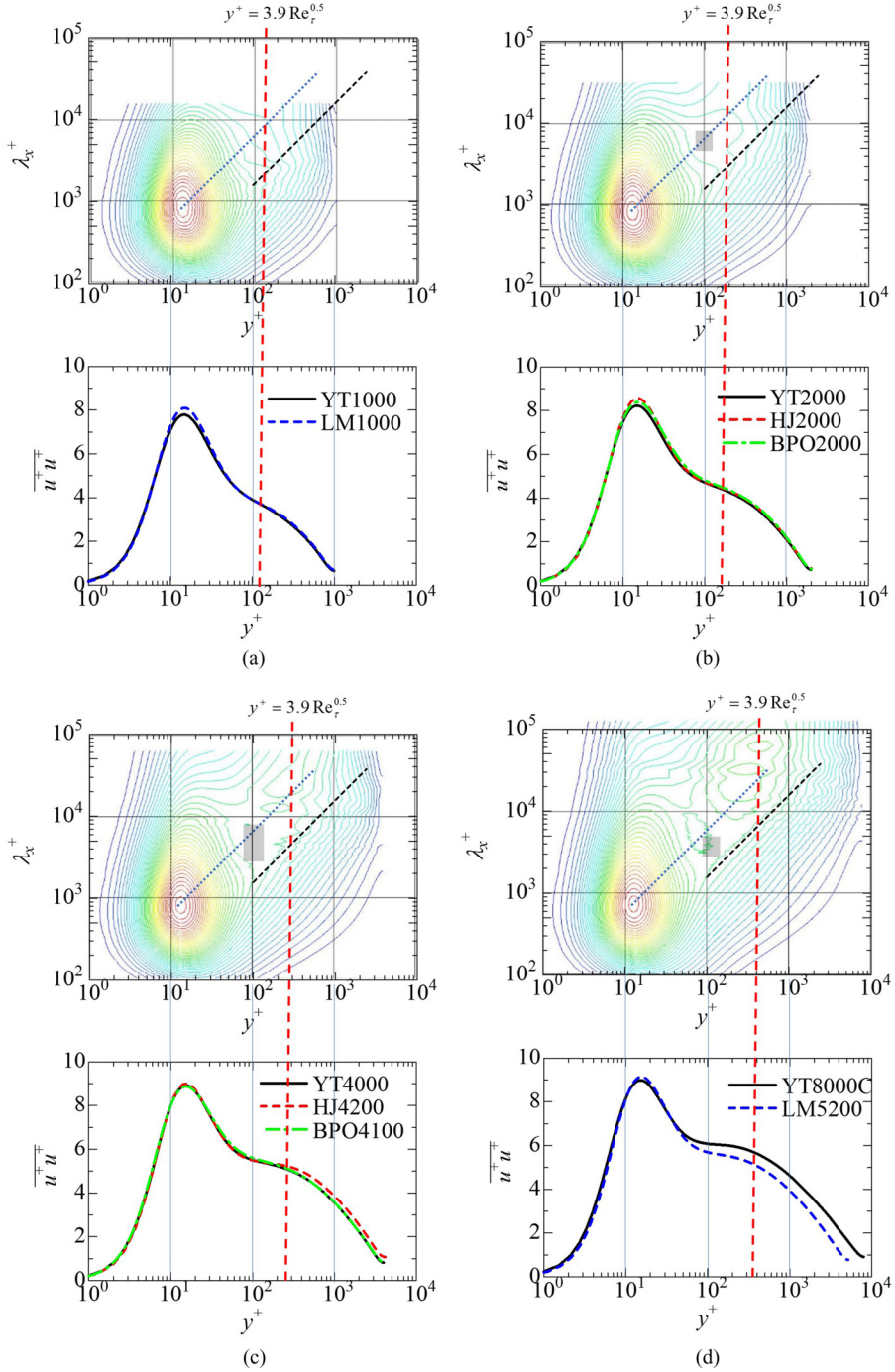


FIG. 5. Contour lines of streamwise premultiplied spectra of  $u$  in the  $y^+ - \lambda_x^+$  plane with profiles of turbulent intensity of  $u$ . Contour maps are lined from 0.1 (blue) to 1.95 (red); spacing in 0.05. Darker-shaded regions denote the  $k_x^{-1}$  regions. Thin broken lines show  $k_x^{-1}$  limits  $\lambda_x = 15.7y$ , from  $y^+ > 100$ . Blue dotted lines denote  $\lambda_x = 100y$  [41]. Red dotted lines denote  $y^+ = 3.9\text{Re}_\tau^{0.5}$  [39,40]. (a)  $\text{Re}_\tau = 1000$ , (b)  $\text{Re}_\tau = 2000$ , (c)  $\text{Re}_\tau = 4000$ , and (d)  $\text{Re}_\tau = 8000$ .

The wavelengths of the first and second peaks in the premultiplied spectrum for the streamwise Reynolds stress are summarized in Table II.

## V. DISCUSSION AND CONCLUSION

Although there have been several experiments and numerical simulations of channel flow, the highest friction Reynolds number is limited to  $Re_\tau = 5900$  by Schultz and Flack [39] and 5200 by Lee and Moser [4] in experiments and simulation, respectively. These Reynolds numbers were not sufficiently high to confirm the logarithmic variation of the streamwise Reynolds stress. In this study, we can confirm the logarithmic variations both in the mean velocity and the streamwise Reynolds stress for  $Re_\tau = 8000$ . This situation is first verified for the present high  $Re_\tau = 8000$  in channel flow. However, their logarithmic regions do not overlap with each other.

The logarithmic mean velocity profile of Eq. (1) is observed between  $300 < y^+ < 1100$  ( $y/h = 0.14$ ). The minimum wall-normal height in the logarithmic region of the streamwise mean velocity corresponded to  $y^+ \approx 3.9Re_\tau^{0.5}$  [40,41] and the second peak of premultiplied spectra is also observed around this wall-normal height [see Fig. 5(d)]. In YT2000 and YT4000 [see Figs. 5(b) and 5(c)], the second peaks of premultiplied spectra are also observed in this wall-normal height with  $y^+ \approx 3.9Re_\tau^{0.5}$ . Hwang [42] reported that the most energetic part of the premultiplied spectra gradually extends to the wall along the linear ridge;  $\lambda_x \approx 100y$ . However, in current DNSs, this trend changes toward the long wavelength with increasing of  $Re_\tau$ .

By contrast, the logarithmic variation of the streamwise Reynolds stress is observed between  $1200$  ( $y/h = 0.15$ )  $< y^+ < 2000$  ( $y/h = 0.25$ ). In Fig. 5, the darker-shaded regions correspond to the  $k_x^{-1}$  law. The  $k_x^{-1}$  law regions are located above the dashed line (black);  $\lambda_x = 15.7y$  [8,12]. As indicated by Agostini and Leschziner [10], the streamwise Reynolds stress in Fig. 5(d) shows the plateau variation between the  $k_x^{-1}$  law and the second peaks of premultiplied spectra regions. To explain the logarithmic and constant portions in the profile of streamwise Reynolds stress, Agostini and Leschziner [10] proposed the modified attached-eddy hypothesis associated with the detached eddies [43].

## ACKNOWLEDGMENTS

The authors are grateful to Dr. N. Furuichi and Dr. Y. Wada for providing their experimental data, and to Prof. J. Philip for his helpful comments on this paper. This research used computational resources of NEC SX-ACE provided by Japan Agency for Marine-Earth Science and Technology (JAMSTEC) and Tohoku University through the HPCI System Research project (Project IDs: hp160173 and hp170195). This research is partially supported by ‘‘Joint Usage/Research Center for Interdisciplinary Large-Scale Information Infrastructures’’ in Japan (Project IDs: jh160045-MDJ and jh170043-MDJ), and by JSPS KAKENHI Grant No. 15K0579.

- 
- [1] C. B. Millikan, A critical discussion of turbulent flows in channels and circular tubes, in *Proceedings of the 5th International Congress for Applied Mechanics* (Wiley, 1938), pp. 386–392.
  - [2] J. P. Monty, Developments in smooth wall turbulent duct flows, Doctoral dissertation, University of Melbourne, Department of Mechanical and Manufacturing Engineering, 2005.
  - [3] H. M. Nagib and K. A. Chauhan, Variations of von Kármán coefficient in canonical flows, *Phys. Fluids* **20**, 10518 (2008).
  - [4] M. Lee and R. D. Moser, Direct numerical simulation of turbulent channel flow up to  $Re_\tau = 5200$ , *J. Fluid Mech.* **774**, 395 (2015).
  - [5] A. A. Townsend, *The Structure of Turbulent Shear Flow* (Cambridge University Press, Cambridge, 1980).

- [6] A. E. Perry, S. Henbest, and M. S. Chong, A theoretical and experimental study of wall turbulence, *J. Fluid Mech.* **165**, 163 (1986).
- [7] A. E. Perr and M. S. Chong, On the mechanism of wall turbulence, *J. Fluid Mech.* **119**, 173 (1982).
- [8] M. Hultmark, M. Vallikivi, S. C. C. Bailey, and A. J. Smits, Turbulent Pipe Flow at Extreme Reynolds Numbers, *Phys. Rev. Lett.* **108**, 094501 (2012).
- [9] I. Marusic, J. P. Monty, M. Hultmark, and A. J. Smits, On the logarithmic region in wall turbulence, *J. Fluid Mech.* **716**, R3 (2013).
- [10] L. Agostini and M. Leschziner, Spectral analysis of near-wall turbulence in channel flow at  $Re_\tau = 4200$  with emphasis on the attached-eddy hypothesis, *Phys. Rev. Fluids* **2**, 014603 (2017).
- [11] A. Lozano-Durán and J. Jiménez, Effect of the computational domain on direct simulations of turbulent channels up to  $Re_\tau = 4200$ , *Phys. Fluids* **26**, 011702 (2014).
- [12] N. Hutchins and I. Marusic, Evidence of very long meandering features in the logarithmic region of turbulent boundary layers, *J. Fluid Mech.* **579**, 1 (2007).
- [13] N. Hutchins, T. B. Nickels, I. Marusic, and M. S. Chong, Hot-wire spatial resolution issues in wall-bounded turbulence, *J. Fluid Mech.* **635**, 103 (2009).
- [14] R. Mathis, N. Hutchins, and I. Marusic, Large-scale amplitude modulation of the small-scale structures in turbulent boundary layers, *J. Fluid Mech.* **628**, 311 (2009).
- [15] M. Hultmark, M. Vallikivi, S. C. C. Bailey, and A. J. Smits, Logarithmic scaling of turbulence in smooth- and rough-wall pipe flow, *J. Fluid Mech.* **728**, 376 (2013).
- [16] B. J. Rosenberg, M. Hultmark, M. Vallikivi, S. C. C. Bailey, and A. J. Smits, Turbulence spectra in smooth- and rough-wall pipe flow at extreme Reynolds numbers, *J. Fluid Mech.* **731**, 46 (2013).
- [17] See <http://www.me.yamanashi.ac.jp/lab/yamamoto/DNS2> for the current DNS statistics.
- [18] Y. Morinishi, T. S. Lund, O. V. Vasilyev, and P. Moin, Fully conservative higher order finite difference schemes for incompressible flow, *J. Comput. Phys.* **143**, 90 (1998).
- [19] W. J. Barrs, N. Hutchins, and I. Marusic, Spectral stochastic estimation of high-Reynolds-number wall-bounded turbulence for a refined inner-outer interaction model, *Phys. Rev. Fluids* **1**, 054406 (2016).
- [20] J. Kim, P. Moin, and R. Moser, Turbulence statistics in fully developed channel flow at low Reynolds number, *J. Fluid Mech.* **177**, 133 (1987).
- [21] S. L. Lyons, T. J. Hanratty, and J. B. McLaughlin, Large-scale computer simulation of fully developed turbulent channel flow with heat transfer, *Int. J. Numer. Methods Fluids* **13**, 999 (1991).
- [22] N. Kasagi, Y. Tomita, and A. Kuroda, Direct numerical simulation of passive scalar field in a turbulent channel flow, *J. Heat Transfer* **114**, 598 (1992).
- [23] R. D. Moser, J. Kim, and N. N. Mansour, Direct numerical simulation of turbulent channel flow up to  $Re_\tau = 590$ , *Phys. Fluids* **11**, 943 (1999).
- [24] J. C. del Alamo, J. Jiménez, P. Zandonade, and R. D. Moser, Scaling of the energy spectra of turbulent channels, *J. Fluid Mech.* **500**, 135 (2004).
- [25] S. Hoyas and J. Jiménez, Scaling of the velocity fluctuations in turbulent channels up to  $Re_\tau = 2003$ , *Phys. Fluids* **18**, 011702 (2006).
- [26] M. Bernardini, S. Pirozzoli, and P. Orlandi, Velocity statistics in turbulent channel flow up to  $Re_\tau = 4000$ , *J. Fluid Mech.* **742**, 171 (2014).
- [27] Y. Yamamoto and T. Kunugi, MHD effects on turbulent dissipation process in channel flows with an imposed wall-normal magnetic field, *Fusion Eng. Des.* **109-111**, 1137 (2016).
- [28] Y. Yamamoto and Y. Tsuji, Effects of large-scale structures on inner layer in high Reynolds number turbulent channel flow, Tenth International Symposium on Turbulence and Shear Flow Phenomena, 2017 (unpublished).
- [29] Y. Yamamoto and Y. Tsuji, Characteristics of overlap region in high-Reynolds number turbulent channel flow, 15th European Turbulence Conference, 2015 (unpublished).
- [30] R. L. Thompson, L. E. B. Sampaio, F. A. de Bragança Alves, L. Thais, and G. Mompean, A methodology to evaluate statistical errors in DNS data of plane channel flows, *Comput. Fluids* **130**, 1 (2016).
- [31] N. Furuichi, Y. Terao, Y. Wada, and Y. Tsuji, Friction factor and mean velocity profile for pipe flow at high Reynolds numbers, *Phys. Fluids* **27**, 095108 (2015).

- [32] Y. Wada, N. Furuichi, Y. Terao, and Y. Tsuji, The experimental study on the turbulent statistics in the outer layer in high Reynolds number turbulent pipe flow, [Trans. JSME](#) **81**, 15 (2015) (in Japanese).
- [33] H. C. H. Ng, J. P. Monty, N. Hutchins, M. S. Chong, and I. Marusic, Comparison of turbulent channel and pipe flows with varying Reynolds number, [Exp. Fluids](#) **51**, 1261 (2011).
- [34] T. B. Nickels, I. Marusic, S. Hafez, and M. S. Chong, Evidence of the  $k_1^{-1}$  Law in a High-Reynolds-Number Turbulent Boundary Layer, [Phys. Rev. Lett.](#) **95**, 074501 (2005).
- [35] S. J. Kline, W. C. Reynolds, F. A. Schraub, and P. W. Runstadler, The structure of turbulent boundary layers, [J. Fluid Mech.](#) **30**, 741 (1967).
- [36] J. Jiménez and A. Pinelli, The autonomous cycle of near-wall turbulence, [J. Fluid Mech.](#) **389**, 335 (1999).
- [37] W. Schoppa and F. Hussain, Coherent structure generation in near-wall turbulence, [J. Fluid Mech.](#) **453**, 57 (2002).
- [38] P. A. Davidson, T. B. Nickels, and P. Å. Krogstad, The logarithmic structure function law in wall-layer turbulence, [J. Fluid Mech.](#) **550**, 51 (2006).
- [39] M. P. Schultz and K. A. Flack, Reynolds-number scaling of turbulent channel flow, [Phys. Fluids](#) **25**, 025104 (2013).
- [40] J. C. Klewicki, Reynolds number dependence, scaling, and dynamics of turbulent boundary layers, [J. Fluids Eng.](#) **132**, 094001 (2010).
- [41] C. Chin, J. Philip, J. Klewicki, A. Ooi, and I. Marusic, Reynolds-number-dependent turbulent inertia and onset of log region in pipe flows, [J. Fluid Mech.](#) **757**, 747 (2014).
- [42] Y. Hwang, Mesolayer of attached eddies in turbulent channel flow, [Phys. Rev. Fluids](#) **1**, 064401 (2016).
- [43] J. Jimenez, Cascades in wall-bounded turbulence, [Annu. Rev. Fluid Mech.](#) **44**, 27 (2011).